BOUNDARY LAYER STUDIES OF MODEL AND FULL-SCALE VTOL INLETS IN THE DIFFUSION LIMITED FLOW REGION

Michael A. Boles

Prepared for

NASA - Lewis Research Center

Under Grant Number NAG3-89

NAG3-89

July 1982

Department of Mechanical and Aerospace Engineering
North Carolina State University
Raleigh, North Carolina 27650

ABSTRACT

This research work provides theoretical verification of the diffusion limit, the ratio maximum surface velocity to diffuser exit surface velocity, for boundary layer flow within VTOL inlets at low weight flows. The effect of model scale size on the diffusion limit is investigated. The theoretical diffusion ratio is shown to lie within the experimental values for the scale model inlets. The full-scale inlet can experience a somewhat larger diffusion ratio than the scale models and still remain separation free.

The application of suction boundary-layer control techniques to VTOL engine nacelle inlets is investigated. A theoretical analysis is employed to determine the optimum amount of suction flow and suction location to achieve high angle-of-attack attached flow at a severe design flow condition of incidence angle free-stream Mach number and throat Mach number. Both 1/3 scale and full-scale model inlets were evaluated in terms of the suction power coefficient, mean suction velocity and percent suction mass flow required to maintain separation-free flow to the diffuser exit.

It was found that the suction location should start in the region of maximum surface velocity and extend down stream for about 15% of surface distance from the highlight to the diffuser exit. It is shown that the full-scale model inlet has improved suction requirements over those of the 1/3 scale model inlet at both the design point and off-design points.

TABLE OF CONTENTS

TABLE OF FIGURES

Page

NOMENCLATURE

C_f	local skin friction coefficient
C_p	specific heat at constant pressure, KJ/Kg°K
C_w	suction power coefficient
D	diameter, m
D_e	exit diameter, m
D_h	highlight diameter, m
D_t	throat diameter, m
L	length, m
M	local Mach number
M_T, M_t	average one-dimensional throat Mach number
M_{max}	maximum local Mach number
M_0	free-stream Mach number
m_f	suction mass flow percent ($\dot{m}_s/\dot{m}_t$ x 100)
$\dot{m}_s$	suction mass flow rate, Kg/s
$\dot{m}_t$	inlet mass flow rate, Kg/s
R	suction location total pressure ratio
S	surface distance from inlet highlight, m
S_{ref}	surface distance from inlet highlight to diffuser exit, m
S_s	surface distance from inlet highlight to location of start of suction, m
ΔS_s	extent of suction, m
$T_{t,0}$	total free-stream temperature, °K
V	velocity, m/s
V_{de}	diffuser exit velocity, m/s
V_{max}	maximum surface velocity, m/s
V_0	free-stream velocity, m/s

V_T, V_t	average throat velocity, m/s
V_{ms}	mean suction velocity, m/s
$\dot{W}_{ref}$	reference power, KW
$\dot{W}_s$	suction power, KW
α	incidence angle, degrees
η_{ad}	adiabatic efficiency
γ	ratio of specific heats

INTRODUCTION

Vertical takeoff and landing multimission aircraft have been of interest to the Navy for a number of years. The Navy has directed its interest in VTOL toward the Type A subsonic aircraft which is capable of operational missions such as antisubmarine warfare, airborne early warning and vertical onboard delivery. An important part of the development of technology for this Navy VTOL aircraft is concerned with the tilting-nacelle lift-cruise fan propulsion systems.

The inlets of these nacelles must operate over a wide range of incidence angles, flight speeds and throttle settings during takeoff and landing, as shown in Figure 1. The inlet design is one of the major concerns for the tilting lift-cruise fan because at large incidence angles the inlet internal flow may separate. The fan-face flow distortion due to separation will cause increased fan blade stress and may cause core-compressor stall.

Experimental and theoretical studies (Refs. 1 to 26) have been conducted to determine the effects of geometry and flow conditions on the performance of engine nacelle inlets for both vertical takeoff and landing aircraft and short-haul aircraft, which will operate at similar, but somewhat less difficult, flow conditions. The experimental performance of the engine inlets is reported in References 1 to 15. Theoretical studies using potential flow and boundary layer analysis are presented in References 6, 8, 9 and 16 to 30.

Engine inlets required to operate under the flight conditions of VTOL aircraft experience increasing incidence angle and throat Mach number.

With these higher surface velocities, greater amounts of deceleration must occur on the inlet surface between the maximum velocity location and the diffuser exit. If the amount of flow deceleration is too great, flow separation may develop (Ref. 20).

To aid in the analysis of a given surface velocity distribution for the possibility of flow separation, Reference 20 recommends nondimensionalizing the local surface velocity by the maximum velocity (local velocity ratio). Flow conditions resulting in the same dimensionless local velocity ratio distribution over the flow surface have the same flow separation characteristics. When the local velocity ratio goes below a certain value (dependent upon conditions prior to diffusion) separation is indicated.

In Reference 21 the concept of Reference 20 is applied in a slightly different manner. Maintaining attached flow throughout the inlet, i.e. to the diffuser exit, is considered to be the design requirement. Therefore, the surface velocities are nondimensionalized by the diffuser exit surface velocity. Then, if the ratio of maximum velocity to diffuser exit velocity (i.e. the diffusion ratio) exceeds a certain value, separation is indicated.

Even though engine inlets proposed for VTOL applications operate at subsonic throat Mach numbers, the Mach number on the inlet internal surface may become locally supersonic and reach Mach numbers as high as 2.0. Based on STOL experimental data, Reference 1 suggests that these supersonic conditions strongly influence the boundary layer separation process through shock/boundary layer interaction. Thus, another parameter, peak Mach number, should be useful for predicting boundary layer separation. The two parameters, diffusion ratio and peak Mach number, were used throughout References 21, 22 and 26 as the separation parameters for inlet analysis.

Rather than performing theoretical boundary layer calculations to determine the values of diffusion ratio and peak Mach number at which the flow separates for various inlet geometries and flow conditions, Reference 21 used experimental data from the tests reported in Reference 2 to determine the limiting values of the separation parameters. The results of this technique are summarized in the following paragraphs.

The experimental flow separation data for the inlets of Reference 2 are illustrated in Figure 2. These data were obtained by setting the free stream Mach and the throat Mach number (inlet mass flow) and then increasing the inlet incidence angle to the point of observed lip separation. The values of diffusion ratio and peak Mach number plotted on Figure 2 are obtained at the incidence angle immediately before the flow separated. These angles (not indicated on the figure) depend upon the flow conditions and may differ from point to point.

Each data point on Figure 2 is a separation limit for its flow condition. In Figure 2(a) peak Mach number curves increase with increasing M_T/M_0 up to a limit. These peak Mach number limits form a band in the range of 1.4 to 1.6. Points lying outside this band are diffusion limited (Fig. 2(b)). These diffusion limits increase somewhat with increasing M_T/M_0 but still lie in a band in the range 2.4 to 2.9. Here, the data points that fell outside the peak Mach number limit band fall within the diffusion limit band.

In summary, at lower throat Mach numbers the separation-free flow appears to be diffusion ratio limited and at higher throat Mach numbers, the separation-free flow appears to be peak Mach number limited.

A major problem in the development of the tilt-nacelle propulsion system is the prediction of the performance characteristics of the inlet

and how these characteristics are affected by scale model size. References 9 and 25 have experimentally attacked the boundary-layer separation problem for both 1/3 scale and full-scale models for a proposed VTOL tilt-nacelle inlet. So far no satisfactory explanation has been found to explain the scale effect of aerodynamic performance characteristics of these inlets.

The studies referenced previously have dealt with the low-speed operational requirements of V/STOL inlets without using boundary-layer control within the inlet. To improve the engine nacelle inlet performance by means other than geometrical considerations, several investigations have considered the use of some means of boundary-layer control within the engine nacelle inlet. Experimental results are presented in Reference 7 for the concept of self-pumping boundary-layer control where a portion of the flow is removed from high pressure regions of the flow and reinjected into lower pressure regions on the inlet internal surface. This system was demonstrated to work and avoids the need for external source of power for the pumping process. References 18, 19 and 20 review analytical methods employed by many investigators for boundary-layer control over aerodynamic surfaces. References 14 and 15 have achieved active boundary-layer control by blowing near the throat of the inlet. These results show marked improvement in the angle-of-attack performance of the inlet as compared to the same inlet with boundary-layer control. The application of active boundary-layer control in the design of optimum subsonic, high-angle-of-attack nacelles is presented by Luidens (Refs. 27 and 28). The concepts of employing boundary-layer control for VTOL aircraft discussed here included suction, blowing and self-pumping. These boundary-layer control techniques may provide a means of optimizing the operational range of a tilting-nacelle VTOL engine.

This report presents the results of a two-part theoretical investigation of the boundary-layer flow within V/STOL engine inlets. First, the theoretical separation bounds and the theoretical diffusion limit are determined for a 1.46 contraction ratio V/STOL inlet. Second, the effects of boundary-layer control by suction in the same V/STOL inlet is studied. Results are presented to show the effect of location and axial extent of the suction opening on the required suction power to maintain separation-free flow at one design operating condition and several off-design conditions.

SEPARATION LIMITS

Method of Analysis

The first part of this study addresses the continued application of the NASA Lewis Subsonic Inlet Boundary-Layer Program (Ref. 29 and 30) to VTOL inlet design. The inlet selected for study is shown in Figure 3. The nomenclature used and the principal inlet geometric variables are illustrated here and a more detailed description is given in Reference 2.

The theoretical potential flow and boundary-layer calculation for the inlet at the various operating conditions was obtained using the calculation procedures for engine inlets presented in Reference 29. The basic elements of the computer program system are (1) a program for geometry definition; (2) an incompressible potential-flow calculation program; (3) a program to combine basic potential-flow solutions into solutions of interest (having specified values of free-stream velocity, incidence angle, and internal mass flow) and also to correct the results for compressibility effects and local supersonic Mach number effects; and, (4) calculations of boundary-layer using the surface Mach number distribution of step (3).

The boundary-layer calculation technique is that given by Reference 30. There a calculation method is described for the numerical solution of the two-dimensional boundary-layer equations. Calculations may be performed with laminar and turbulent flow including transition for arbitrary Reynolds number and free-stream velocity distribution on planar or axisymmetric bodies with transpiration. The boundary-layer program calculates boundary-layer profiles, displacement thickness, skin friction coefficient C_f, etc. at each station along the body starting from the stagnation point. In this

study transition is forced to fully turbulent flow at the maximum surface velocity if the program has not predicted transition to turbulent flow at this point.

There are some shortcomings of this computational method. First, the flow about an inlet at non-zero incidence angle is truly three-dimensional, thus the axisymmetric flow assumption neglects any secondary flow about the inlet. Second, for many cases of interest having various incidence angles, free-stream velocities and throat Mach number (inlet mass flow) the inlet surface may experience regions of local supersonic flow. Thus, it may be necessary to account for possible shock-boundary-layer interaction in the boundary-layer calculations which the current calculation method cannot do. Also, the transition model does not account for separation bubbles that appear in some of the experimental data. However, comparisons of results from this analytical method show good agreement with the separation bounds predicted by experimental data (Refs. 5 and 8).

RESULTS AND DISCUSSION

Theoretical boundary-layer calculations using the above procedures were performed to determine the values of the diffusion ratio and peak Mach number at which the flow separates for the inlet shown in Figure 3. These calculations were made for 1/5 scale, 1/3 scale and full-scale models (for full-scale, D_e = 152.4 cm) at two values of free-stream Mach number and a range of values of throat Mach number and inlet incidence angle. Theoretical separation bounds are presented and the separation parameters, the diffusion ratio, V_{max}/V_{de}, and peak Mach number, M_{max}, are compared to the experimental separation limits. All flow results are shown for the windward (see Fig. 3) side of the inlet since the

most severe flow conditions occur at this position.

Figure 4 illustrates the method used to determine the separation boundary for the three 1.46 contraction ratio model inlets. This figure presents the effect of incidence angle on the surface Mach number and local skin friction coefficient at a free-stream Mach number of 0.18 and a throat Mach number of 0.27 for the 1/3 scale model inlet. Figure 4(a) gives the surface Mach number distribution for these conditions. As the incidence angle is increased, from 35^{o} to 65^{o}, the peak surface Mach number increases and moves from an internal lip location to a location just outside the highlight on the external lip. Figure 4(b) gives the local skin friction coefficient as a function of dimensionless surface distance from the highlight at these same flow conditions. Here, the curve for incidence angle of 35^{o} illustrates attached flow to the diffuser exit while the curves for 50^{o} and 65^{o} are examples of diffuser separation and indicate the movement of the separation location from the diffuser exit toward the lip section. On Figure 4(b), the skin friction coefficient curves show a transition from laminar to turbulent flow. At incidence angle of 35^{o} the peak surface Mach number occurs at a dimensionless surface location of 0.035 and the flow undergoes transition from laminar to turbulent flow and the flow remains attached to the diffuser exit. At incidence angles of 50^{o} and 65^{o}, the peak Mach number occurs just outside the highlight and the boundary-layer calculations were forced to transition to turbulent flow at this point. At 50^{o} incidence angle the separation point is at a dimensionless distance of 0.278 and at 65^{o} the location has moved to a dimensionless distance of 0.207 which is also the throat location for this inlet.

These calculations can be repeated to determine the incidence angle for the onset of diffuser separation at a given free-stream Mach number and throat Mach number. By varying the throat Mach numbers at fixed free-stream Mach numbers, the separation bounds for the three-scale model inlets can be determined. The results of these calculations are shown in Figure 5. Figures 5(a) and 5(b) give the separation boundary for the 0.12 and 0.18 free-stream Mach numbers, respectively. These results illustrate the effect of model scale or Reynolds number on the theoretical separation boundary. At both of the free-stream Mach numbers investigated, the full-scale inlet demonstrated a wider separation free operating range than the 1/5 or 1/3 scale model inlets. The 1/3 scale model inlet shows a wider separation free operation range than the 1/5 scale model inlet at the free-stream Mach number of 0.12; however, at 0.18 free-stream Mach number the separation boundary is essentially the same for these two scale models.

The theoretical diffusion ratio and peak Mach number separation results for these inlets are illustrated in Figure 6. The values of the velocity diffusion ratio, V_{max}/V_{de}, and peak Mach number, M_{max}, plotted on Figure 6 were obtained at the incidence angle flow conditions of Figure 5. The regions above the individual curves of Figure 6 represent separated flow and the regions below each curve are for attached flow.

Figure 6(a) shows that as the average throat Mach number (consequently M_T/M_o for fixed M_o) is increased, the peak Mach number increases to some maximum value; only for the 1/5 scale model inlet at 0.12 free-stream Mach number has the peak Mach number reached a maximum value for the flow conditions investigated. The other scale model inlets for these flow conditions (except the full-scale at 0.18 free-stream Mach number) appear to be approaching their maximum peak Mach numbers. Included on

Figure 6(a) is the experimental separation boundary from Reference 21. Good correlation between the experimental and theoretical peak Mach number limit is exhibited for the 1/5 scale model inlet.

Figure 6(b) shows that as throat Mach number (consequently M_T/M_0 for fixed M_0) is decreased from its maximum value for each curve, the diffusion ratio increases up to a point and then decreases at lower throat Mach numbers. This behavior establishes the theoretical upper limit on the diffusion ratio above which the flow separates at the lower throat Mach numbers. Included on Figure 6(b) is the experimental diffusion limit from Reference 21. Both the 1/5 and 1/3 scale model inlets have theoretical diffusion ratios which lie within the experimental range of the 1/5 scale model inlet of 2.4 to 2.9. The full-scale model inlet has a larger value for the theoretical diffusion ratio than the smaller scale model inlets and the value is in the range of 2.8 to 3.3 for this inlet geometry.

In summary, at lower throat Mach numbers, the boundary-layer flow in scale model VTOL engine inlets is diffusion limited with the theoretical limit range being approximately equal to that predicted by the experimental data. The full-scale inlet exhibits a somewhat higher value of the diffusion limit due to scale or Reynolds number effects.

BOUNDARY-LAYER CONTROL BY SUCTION

Method of Solution

The second part of this study investigates the option of active boundary-layer control by suction as a means to provide attached flow to the diffuser exit or fan of tilting-nacelle VTOL engine inlets. The effects of boundary-layer control by suction in the VTOL inlet studied here will be limited to the low throat Mach number (low weight flow), diffusion limited separation region. The effort is directed to determining

the dependence of boundary-layer control by suction on incidence angle, throat Mach number and free-stream velocity for attached flow to the diffuser exit. The goal is to expand the operation region of the inlet as shown in Figure 5. Here the theoretical separation boundary for the 1.46-contraction-ratio-model-scale and full-scale inlet is shown. The region below this boundary represents attached flow conditions. This investigation will be limited to the 1/3 scale model and full-scale inlets as shown in Figure 3. The effect of suction location and suction slot extent will be evaluated in terms of the power, percent of total inlet mass flow and mean suction to average throat velocity ratio required for attached flow to the diffuser exit.

Selection of Design Flow Condition

Representative incidence angle, throat Mach number (inlet mass flow) and free-stream Mach number during takeoff and landing are shown in Figure 1. Similar data obtained from Reference 11 for a subsonic, VSTOL, tilt-nacelle aircraft, with and without a jet deflection vane in the exhaust jet, were interpreted in terms of parameters pertinent to inlet aerodynamics by Reference 26 and are presented here as Figure 7 (solid lines). These data are compared with the experimental separation bound for the 1.46-contraction-ratio inlet (dashed line) from Reference 2.

Based on Figure 7, a typically severe flow condition (the data symbol) was selected for analysis. This condition occurred at a free-stream Mach number of 0.18, an incidence angle of 70° and a throat Mach number of 0.27.

The potential flow surface Mach number distribution and variation in separation location for the 1/3 scale model and full-scale inlets for flow conditions about the selected deisgn point are shown in Figures 8, 9 and 10. Figure 8 gives the surface Mach number distribution for the design

point at an incidence angle of 70^0, free-stream Mach number of 0.18 and throat Mach number of 0.27. This Mach number distribution, plotted against the dimensionless surface distance, is valid for both the 1/3 scale model and full scale inlet. Since the flow at this design point has a diffusion ratio of V_{max}/V_{de} of 4.8 and a peak Mach number of 1.15, the flow for both the 1/3 scale model and full scale inlet are in diffusion limited separation region discussed in Part I of this report. The separation location for the 1/3 scale model is at a dimensionless surface location of 0.195, a point just upstream of the throat on the internal lip; and the separation location for the full scale inlet is at a dimensionless surface location of 0.222, a point just downstream of the throat in the diffuser section.

Figure 9 summarizes the results shown on Figure 8 for conditions about the design point. On Figure 9(a) the dimensionless separation location (determined as the surface location where the local skin friction coefficient is zero) is plotted against the average throat Mach number at an incidence angle of 70^0 and free-stream Mach number of 0.18 for both the 1/3 scale model and full scale inlets. As the average throat Mach number is decreased the separation point moves from the diffuser exit, S/S_{ref} of 1, toward the highlight. The effects of scale on the separation location can be observed from this figure. The full scale inlet exhibits more delayed separation characteristics than did the 1/3 scale model inlet. However, for throat Mach numbers below the design point (M_T = 0.27) the full scale inlet exhibits separation characteristics very near that of the 1/3 scale model inlet. Both inlets experience separation at the highlight location for the lowest values of the throat Mach number. This is similar to the experimental separation characteristics observed by Reference 25.

Figure 9(b) shows the effect of increasing incidence angle on the separation location for the model and full-scale inlets at an average throat Mach number of 0.27 and a free-stream Mach number of 0.18. Here the full-scale inlet has better separation characteristics than the model inlet up to an incidence angle of approximately 70^{o}. From 70^{o} to 90^{o} incidence angle the separation location of the full-scale and 1/3 scale model inlets are very nearly equal.

For completeness at this point, Figure 10 is included to illustrate the effect of free-stream Mach number of 0.12 on the separation location for the 1/3 scale model and full-scale inlets. On Figure 10(a) is plotted the separation location versus the average throat Mach number at an incidence angle of 70^{o} and the free-stream Mach number of 0.12. As the average throat Mach number is decreased the separation point moves from the diffuser exit toward the highlight. These results are similar to those discussed for Figure 9(a); however, the separation location does not progress to the highlight for either of the inlets as in the free-stream Mach number of 0.18 case. Figure 10(b) shows the variation of the separation location with increasing incidence angle. Here, as in Figure 9(b), the full-scale inlet exhibits improved separation characteristics over the 1/3 scale model inlet. Figures 9 and 10 illustrate that at an incidence angle of 70^{o} and average throat Mach number of 0.27, the free-stream Mach number of 0.18 gives a more severe operation condition than a free-stream Mach number of 0.12.

Suction Power

A VTOL engine inlet suction boundary-layer control system is shown in Figure 11. The figure shows the suction surface and the pump required to pump the suction air. It is assumed that the suction pump

restores the total head of the suction air to that of the free-stream, discharging it with a velocity equal to the free-stream velocity.

The inlet flow begins at the stagnation point, first accelerates to the maximum velocity, then diffuses and proceeds to the suction location. The suction location must begin at least at or prior to the boundary-layer separation location for the flow condition. For the selected design point the separation point as determined from Figure 9 is at S/S_{ref} = 0.195 for the model scale and 0.222 for the full-scale inlet. Thus, for the design point, the suction location, S_s, is varied from the highlight location to S/S_{ref} of 0.184 for the scale model and 0.20 for the full scale-inlet. The extent of the suction, $\Delta S_s/S_{ref}$, is varied from 0.05 to 0.30. The suction extent is assumed to extend 60° either side of the windward plane.

The suction power required to maintain attached flow to the fan location is dependent upon not only the inlet flow conditions but also the suction location, extent and mean suction velocity. The suction power required by the pump for attached flow to the fan location is that power needed to remove the required mass flow at the inlet surface and pump it back to the free-stream total pressure and in the downstream direction, resulting in no thrust or drag. If it is assumed that the boundary layer is removed through an ideal porous material covering the suction slot, the plenum chamber static pressure may be assumed to be the same as that at the beginning of the suction location. The suction power may be expressed as

$$\dot{W}_s = \frac{\dot{m}_s \, c_p \, T_{t,0} \left(1 - R^{\frac{\gamma-1}{\gamma}}\right)}{\eta_{ad}}$$

where

$\dot{W}_s$ = suction power

$\dot{m}_s$ = suction mass flow rate

$T_{t,0}$ = total free-stream temperature

c_p = specific heat

R = suction location total pressure ratio

η_{ad} = adiabatic efficiency

γ = ratio of specific heats

A suction power coefficient is defined as the ratio of the suction power to a reference power calculated at the inlet throat conditions. The reference power, $\dot{W}_{ref}$, is given as

$$\dot{W}_{ref} = \frac{\dot{m}_T \, c_p \, T_{t,0}}{\eta_{ad}}$$

where $\dot{m}_T$ is the inlet mass flow rate. The suction power coefficient is now given as

$$C_w = \frac{\dot{m}_s}{\dot{m}_T} (1 - R^{\frac{\gamma-1}{\gamma}})$$

or

$$C_w = m_f (1 - R^{\frac{\gamma-1}{\gamma}}) \times 10^2$$

where m_f is the suction mass flow to inlet mass flow ratio expressed as a percent, called the suction mass flow percent.

Calculation Procedure

To determine the suction power coefficient to maintain attached flow to the diffuser exit, the following procedure was established at the required grid point representing the inlet surface. At each grid point covered by the extent of suction distance, ΔS_s, extending downstream from the suction location, a constant suction flow Mach number

was specified and the free-stream Mach number at each grid point was obtained from the potential flow solution. Then the following parameters were calculated, suction total pressure ration, R; the percent of total inlet mass flow removed by suction called the percent suction mass flow, m_f; the suction power coefficient, C_W; and the ratio of the mean suction velocity to the average throat velocity called the mean suction velocity ratio, V_{ms}/V_T.

The assumption of a constant suction flow Mach number along the suction extent is an idealized assumption. Since the potential flow surface velocity varies over the suction extent, this assumption results in a variable suction total pressure ratio along the suction extent. Thus, the plenum chamber is idealized to be one composed of several smaller plenum chambers, each having its own pressure ratio, suction power and fraction of total mass passing through it. The suction power coefficient and percent suction mass flow reported here are the sums of these parameters over the specified suction extent.

Suction Results and Discussion

In this section the results for suction boundary-layer control are presented for the 1/3 scale model and full-scale inlet at the design flow condition and selected off-design points. The results are presented as plots of the suction power coefficient, mean suction velocity ratio and percent suction mass flow, all as functions of the suction location and extent. Also, typical skin friction coefficient plots are included for discussion. As in the first part of this report, the boundary-layer calculations assumed that transition to turbulent flow occurred at the maximum surface velocity from the potential flow solution for the flow conditions.

Figure 12 shows the variation of the skin friction coefficient along the inlet surface for the 1/3 scale model and full-scale inlet

at the design flow condition (incidence angle of 70°, throat Mach number of 0.27 and free-stream Mach number of 0.18) for suction starting at the highlight location S_s/S_{ref} of 0 and suction extending a dimensionless distance $\Delta S_s/S_{ref}$ of 0.15. These curves were obtained by specifing a constant suction Mach number along the suction extent and then increasing this constant value until the boundary layer remains attached to the diffuser exit. Included on the figures are the calculated values of the suction power coefficient, C_w, mean suction velocity ratio, V_{ms}/V_T, and percent suction mass flow, m_f. On Figure 12(a) the plot of the local skin friction coefficient for the no-suction case indicates separation occurs at $S/S_{ref} = 0.195$ for the 1/3 scale model inlet (also see Figure 8). As the suction Mach number is increased, the skin friction coefficient is increased in the suction region to a sufficient level such that during continued diffusion of the flow from the end of suction to the fan location the boundary layer remains attached. The amount of suction was increased to the point that the skin friction coefficient was non-zero along the inlet surface. Figure 12(b) presents similar results for the full-scale inlet at the same conditions as the 1/3 scale model inlet. Attention is drawn to the fact that the suction parameters for the full-scale inlet are reduced (better) from those required for the 1/3 scale inlet to maintain separation-free flow to the diffuser exit.

Results similar to those illustrated in Figure 12 were obtained at other combinations of suction location and suction extent. Figure 13 is a plot of suction power coefficient, mean suction velocity and percent suction mass flow required to maintain separation-free flow to the diffuser exit as a function of suction extent, $\Delta S_s/S_{ref}$, and suction location, S_s/S_{ref}, for the 1/3 scale model and full-scale inlets at the design flow condition. In general, the results shown in Figure 13 indicate that for the most effective

suction, the suction should be arranged with a suction location starting at the highlight and extending for a suction extent, $\Delta S_s/S_{ref}$ of 0.15. Thus, the most effective suction location is in the region of the strong pressure rise downstream of the maximum velocity (see Figure 8).

The results shown in Figure 13(a) are now discussed in some detail. For suction locations between the highlight, S_s/S_{ref} of 0 and the location, S_s/S_{ref} of 0.15 increasing the suction extent results in a decreasing suction power coefficient and the mean suction velocity required for attached flow to the diffuser exit. However, the percent suction mass flow required for attached flow at first decreases to a minimum value and then begins to increase as the suction extent increases at a fixed suction location. For a given suction location the suction pressure ratio is increasing as the suction extent increases, thus, the work per unit suction mass is decreasing and a lower suction velocity is required for attached flow. But as the suction extent increases, the suction area increases; this results in an increase in the total mass flow required to maintain separation-free flow.

As the suction extent is decreased below 0.15, the suction power coefficient increases dramatically for the suction location, S_s/S_{ref} of 0, 0.5 and 0.1. This is due to the suction being concentrated in the region of maximum surface velocities (see Figure 8) where the suction work per unit suction mass is increasing due to a decreased suction pressure ratio. Here the mean suction velocity and percent suction mass flow increase to maintain attached flow to the diffuser exit. For suction locations near the highlight, using small suction extents resulted in suction parameters that exceeded the range of validity of the boundary-layer program; thus, narrow suction extents could not be fully evaluated with the present calculation techniques.

For suction locations of 0.15 and 0.184, reducing the extent of suction also results in increasing suction power coefficient at the minimum suction extent for attached flow to the diffuser exit is less

than that required at the suction location, S_s/S_{ref}, of 0.10. Here the mean suction velocity increases and the percent suction mass flow decreases with decreasing suction extent; however, the overall levels for these two parameters are increased over those for the smaller suction locations. In this region the work per unit suction is lower because of the decreased surface velocity and thus, increased suction pressure ratio; but, since the suction location is near the separation point, the required percent suction mass flow is increased over that at suction locations nearer the highlight.

Figure 13(b) presents results similar to those of Figure 13(a) except for the full-scale inlet. The suction parameters for the full-scale inlet are reduced (better) from those required for the 1/3 scale inlet to maintain separation-free flow to the diffuser exit. Again, the suction parameters indicate that for the full-scale inlet the most effective suction for minimum power is that which is located in the region of strong pressure rise downstream of the maximum velocity.

The effect of operation at flow conditions other than the design condition of incidence angle of 70°, free-stream Mach number of 0.18 and throat Mach number of 0.27 were investigated for both the 1/3 scale and full-scale inlets. Figure 14 illustrates the effect of increased incidence angle at free-stream Mach numbers of 0.18 and 0.12 at a suction location of S_s/S_{ref} of 0.15 and suction extent of 0.10 and 0.20 for the 1/3 scale and full-scale models. Figure 14(a) plots the result for the free-stream Mach number of 0.18 and Figure 14(b) is for the free-stream Mach number of 0.12. In both figures it is seen that increased suction power coefficients are required for increased incidence angles. Comparison of Figures 14(a) and 14(b) show the effect of free-stream Mach

number. For a fixed value of the suction power coefficient, a larger value of incidence angle may be attained for a selected suction extent. For example, at a throat Mach number of 0.27, suction location of 0.15 and suction extent of 0.20, a suction power coefficient of $1x10^{-4}$ for the 1/3 scale model inlet would have attached flow up to an incidence angle of 50° at a free-stream Mach number of 0.18. While at a free-stream Mach number of 0.12, the same suction power coefficient would allow separation-free flow to an incidence angle of 70°. Figure 14 also illustrates that lower suction values are required for separation-free flow for the full-scale inlet as compared to the 1/3 scale model inlet at increased incidence angles for both free-stream Mach numbers.

The effect of throat Mach number on the incidence angle as a function of the suction power coefficient for separation-free flow for the 1/3 scale model inlet at a suction extent of 0.15, free-stream Mach number of 0.18, and suction locations of 0 and 0.1 at throat Mach numbers of 0.27 and 0.4 are shown on Figure 15. For a fixed suction power coefficient the incidence angle can be increased for increased throat Mach number. The near optimum suction placement of the suction location, S_s/S_{ref}, of 0 and suction extent, $\Delta S_s/S_{ref}$, of 0.15 is also illustrated. For a fixed value of the suction power coefficient, the largest value of the incidence angle for separation-free flow for throat Mach numbers of 0.27 and 0.4 can be achieved at the suction location, S_s/S_{ref}, of 0 rather than a value of 0.10. The observations from Figure 13(a) also apply at elevated throat Mach number and incidence angle.

SUMMARY OF RESULTS

The theoretical separation bounds and theoretical diffusion limit for a 1.46 contraction ratio V/STOL engine inlet was determined and

compared to the experimentally determined values. The theoretical diffusion limit for the 1/5 and 1/3 scale model inlets was found to lie within the experimental limit of diffusion ratio, V_{max}/V_{de} of 2.4 to 2.9 obtained for the 1/5 scale model inlet. The full-scale inlet can withstand a somewhat larger value of the diffusion ratio and maintain separation-free flow. Generally the location of the separation point for the full-scale inlet occurs at a larger surface distance from the highlight location than for the scale model inlet. However, as the average throat Mach number decreases and the free-stream Mach number increases, the improved separation characteristics of the full-scale inlet over the 1/3 scale model inlet are diminished.

The application of suction as a boundary-layer control technique was investigated for ideal suction. The optimum suction location for minimum suction power coefficient and percent suction mass flow occurs when the suction starts near the maximum surface velocity and extends for a distance of about 15% of the surface distance from the highlight to the diffuser exit. When the suction location is near the separation point, strong suction over a suction extent of 5% to 10% of the distance from the highlight to the diffuser exit results in lower suction power coefficient than when the same extents are used for suction locations near the highlight. The full-scale inlet experienced improved suction parameters over the 1/3 scale model inlet.

REFERENCES

1. Jakubowski, A. K.; and Luidens, R. W.: Internal Cowl-Separation at High Incidence Angles. AIAA Paper 75-64, Jan. 1975.

2. Miller, B.; Dastoli, B. J.; and Wesoky, H. L.: Effect of Entry-Lip Design on Aerodynamics and Acoustics of High-Throat-Mach-Number Inlets for the Quiet, Clean, Short-Haul Experimental Engine. NASA TM X-3222, 1975.

3. Hancock, J. P.; and Hinson, B. L.: Inlet Development for the L-500. AIAA Paper 69-448, June 1969.

4. Albers, J. A.: Theoretical and Wxperimental Internal Flow Characteristics of a 13.97 Centimeter-Diameter Inlet at STOL Takeoff and Approach Conditions. NASA TN D-7185, 1973.

5. Felderman, E.; and Albers, J. A.: Comparison of Experimental and Theoretical Boundary-Layer Separation for Inlets at Incidence Angle at Low-Speed-Conditions. NASA TM X-3194, 1975.

6. Albers, J. A.; Stockman, N. O.; and Hirn, J. J.: Aerodynamic Analysis of Several High-Throat-Mach-Number Inlets for the Quiet, Clean, Short-Haul Experimental Engine. NASA TM X-3183, 1975.

7. Miller, B. A.: A Novel Concept for Subsonic Inlet Boundary-Layer Control. Journal of Aircraft, Vol. 14, No. 4, pp. 403-404, April 1977.

8. Chou, D. C.; Luidens, R. W.; and Stockman, N. O.: Prediction of Laminar and Turbulent Boundary-Layer Flow Separation in V/STOL Engine Inlets. NASA TM X-73575, 1977.

9. Koncsek, J.; and Syberg, J.: Fan Inlet for a V/STOL Airplane. AIAA Paper 77-802, July 1977.

10. Smith, E. G.: Propulsion Designed for V/STOL. AIAA Paper No. 77-804, July 1977.

11. Potonides, H. C.; Cea, R. A.; and Nelson, T. F.: Design and Experimental Studies of a Type A V/STOL Inlet. AIAA Paper No. 78-956, July 1978.

12. McCormick, B.: A Critical Look at V/STOL Technology. AIAA Paper No. 78-1526, August 1978.

13. Shaw, A. W.; Lindbeck, R. K.; Craig, S. J.; and Booth, G.: The Impact of Current V/STOL Flying Quality Control Requirements on the Propulsion System. AIAA Paper No. 78-924, July 1978.

14. Burley, R. R.; Johns, A. L.; and Diedrich, J. H.: Subsonic VTOL Inlet Experimental Results. In Proceedings of a Workshop on V/STOL Aircraft Aerodynamics, Naval Post Graduate School, Monterey, CA, May 16-18, 1979, Vol. 11, pp. 648-664.

15. Johns, A. L.; Williams, R. C.; and Potonides, H. C.: Performance of a V/STOL Tilt-Nacelle Inlet with Blowing Boundary-Layer Control. AIAA Paper No. 79-1163, 1979.

16. Albers, J. A.; and Miller, B. A.: Effect of Subsonic Inlet Lip Geometry on Predicted Surface and Flow Mach Number Distributions. NASA TN D-7446, 1973.

17. Albers, J. A.; and Felderman, D. J.: Boundary Layer Analysis of Subsonic Inlet Diffuser Geometries for Engine Nacelles. NASA TN D-7520, 1974.

18. Williams, J.; and Butler, S. F. J.: Aerodynamic Aspects of Boundary-Layer Control for High Lift at Low Speeds. Journal of The Royal Aeronautical Society, April 1963, Vol. 67, No. 628, pp. 201-223.

19. Chang, P. K.: Control of Flow Separation, McGraw-Hill Publishing Company, New York, New York, 1976.

20. Smith, A. M. O.: High-Lift Aerodynamics. Journal of Aircraft, Vol. 12, 1975, pp. 501-530.

21. Boles, M. A.; and Stockman, N. O.: Use of Experimental Separation Limits in the Theoretical Design of V/STOL Inlets. AIAA Paper No. 77-878, July 1977.

22. Boles, M. A.; Luidens, R. W.; and Stockman, N. O.: Theoretical Flow Characteristics of Inlets for Tilting-Nacelle VTOL Aircraft. NASA Technical Paper 1205, 1978.

23. Chou, D. C.; Luidens, R. W.; and Stockman, N. O.: Prediction of Laminar and Turbulent Boundary Layer Flow Separation in V/STOL Engine Inlets. NASA TM X-73575, 1977.

24. Chou, D. C.; Lee, H. C.; Luidens, R. W.; and Stockman, N. O.: Methods for Calculating the Transonic Boundary Layer Separation for V/STOL Inlets at High Incidence Angles. AIAA Paper 78-1340, 1978.

25. Syberg, J.: Inlet Operating Characteristics at High Angles of Attack. To be published.

26. Hawk, J. D.; and Stockman, N. O.: Theoretical Study of VTOL Tilt-Nacelle Axisymmetric Inlet Geometries. NASA TP-1380, January 1979.

27. Luidens, R. W.; Stockman, N. O.; and Diedrich, J. H.: An Approach to Optimum Subsonic Inlet Design. ASME Paper No. 79-FT-51, 1979.

28. Luidens, R. W.; Stockman, N. O.; and Diedrich, J. H.: Optimum Subsonic, High-Angle-of-Attack Nacelles. NASA TM 81491, 1980.

29. Stockman, N. O.: Potential and Viscous Flow in VTOL, STOL, or CTOL Propulsion System Inlets. AIAA Paper 75-1186, Oct. 1975.

30. Herring, J. H.: PL2 - A Calculation Method for Two-Dimensional Boundary Layers with Crossflow and Heat Transfer. NASA Contract Number NAS3-21810, June 1981.

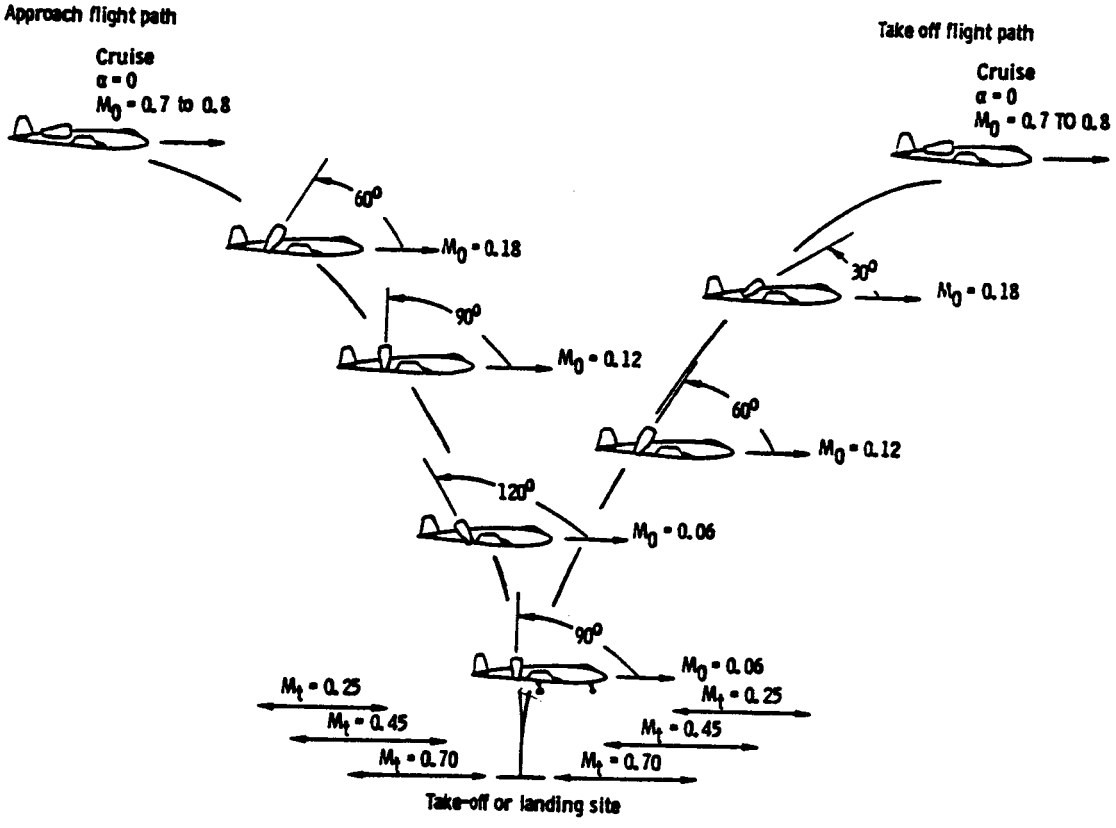

Figure 1. Representative flight conditions for tilt-nacelle VTOL aircraft.

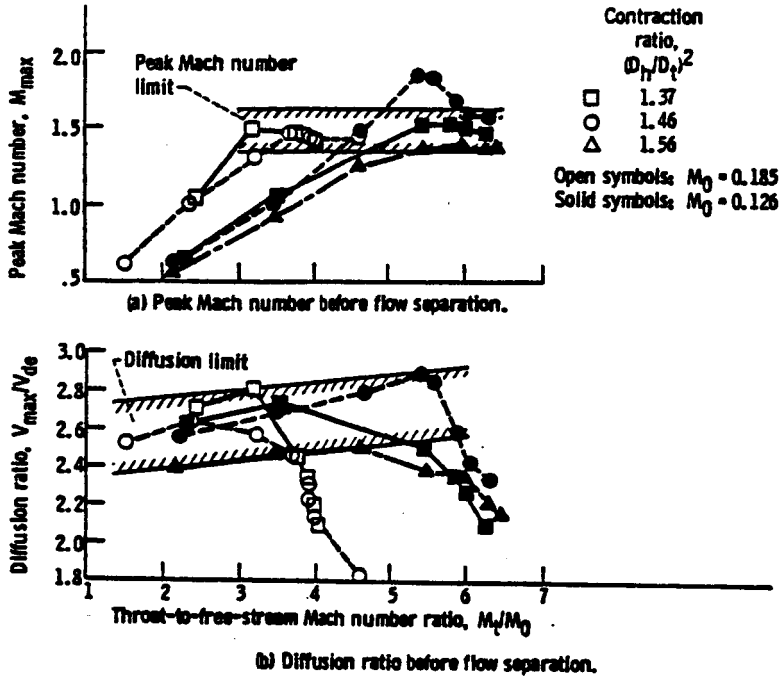

Figure 2. Experimental separation data for STOL inlets (from Ref. 21).

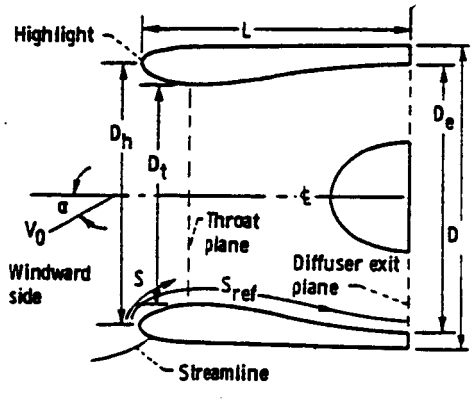

AREA CONTRACTION RATIO $(D_h/D_t)^2 = 1.46$

$D/D_e = 1.111$ $L/D = 1$

FULL SCALE $D_e = 152.4$ cm

Figure 3. Inlet geometry.

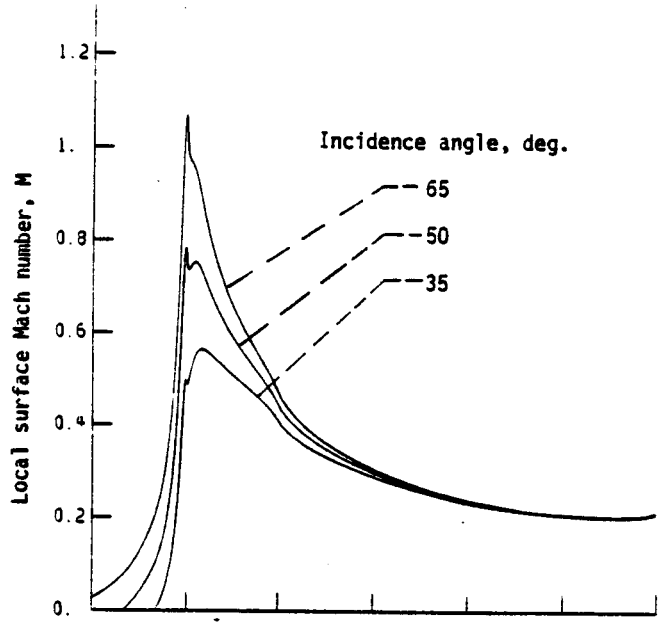

(a) Theoretical local Mach number distribution

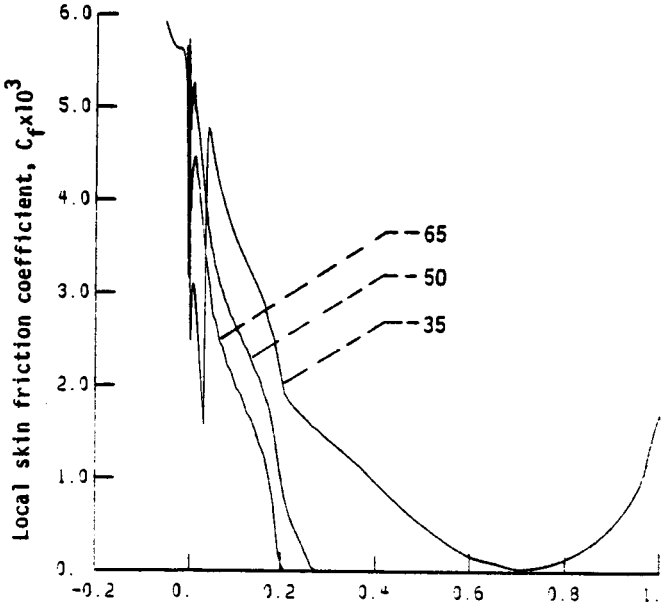

(b) Theoretical local skin friction coefficient

Figure 4. Effect of incidence angle on 1/3 scale model inlet flow separation. Windward side of inlet. $M_0 = 0.18$, $M_T = 0.27$.

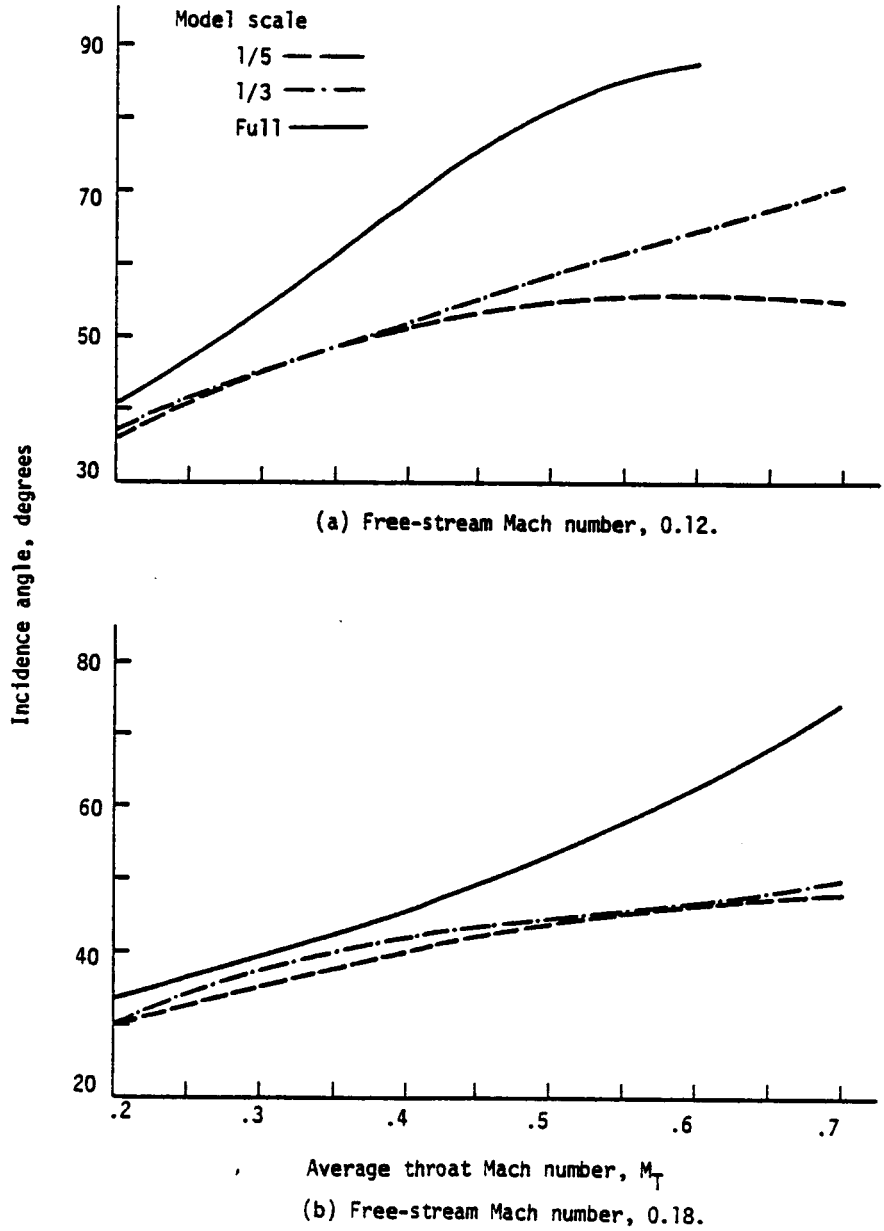

Figure 5. Theoretical incidence angle at flow separation variation with average throat Mach number for 1/5, 1/3 and full-scale inlets. M_0 = 0.12 and 0.18.

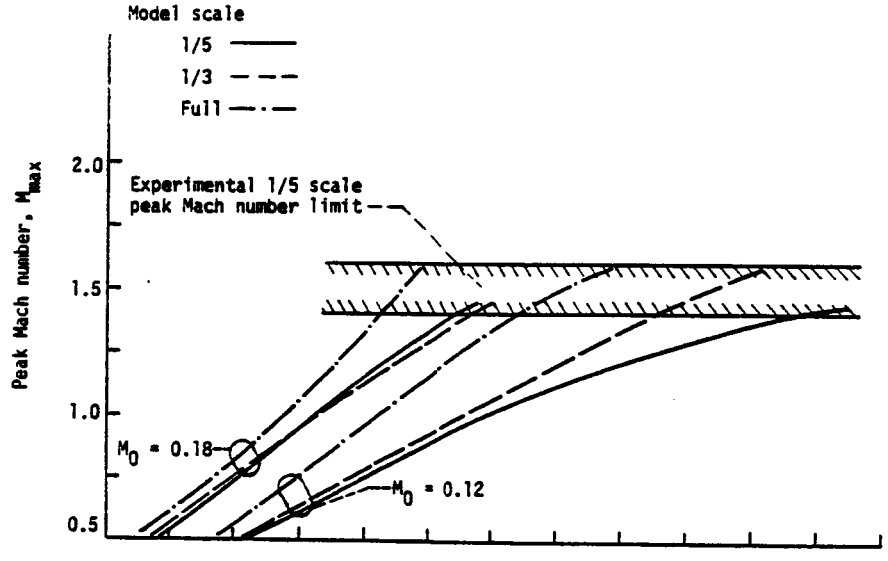

(a) Peak Mach number before flow separation

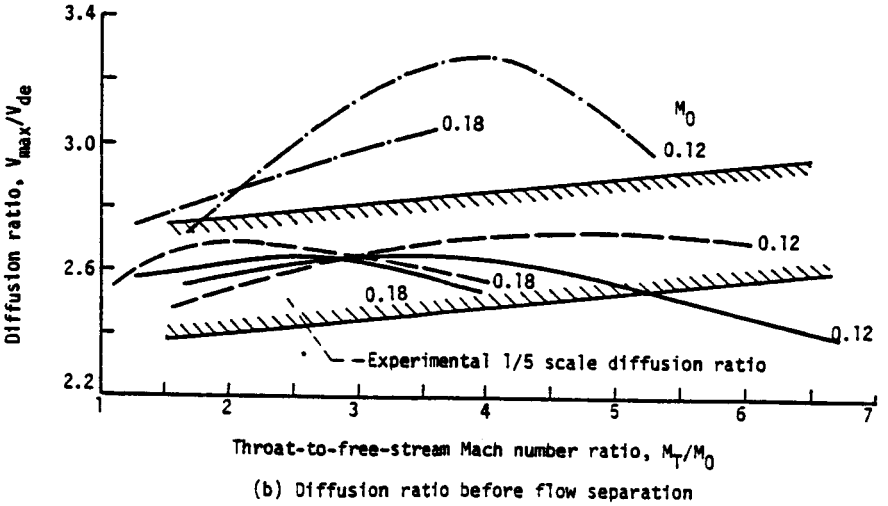

(b) Diffusion ratio before flow separation

Figure 6. Theoretical separation data for 1/5, 1/3 and full-scale inlets.

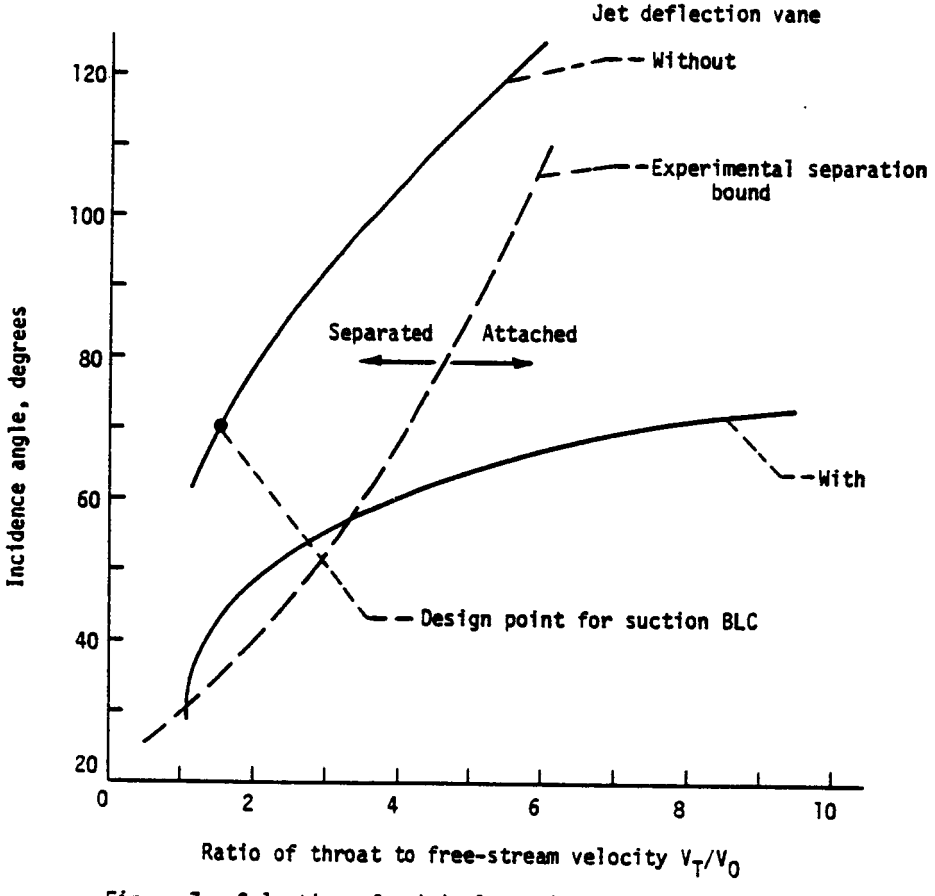

Figure 7. Selection of critical condition for inlet analysis.

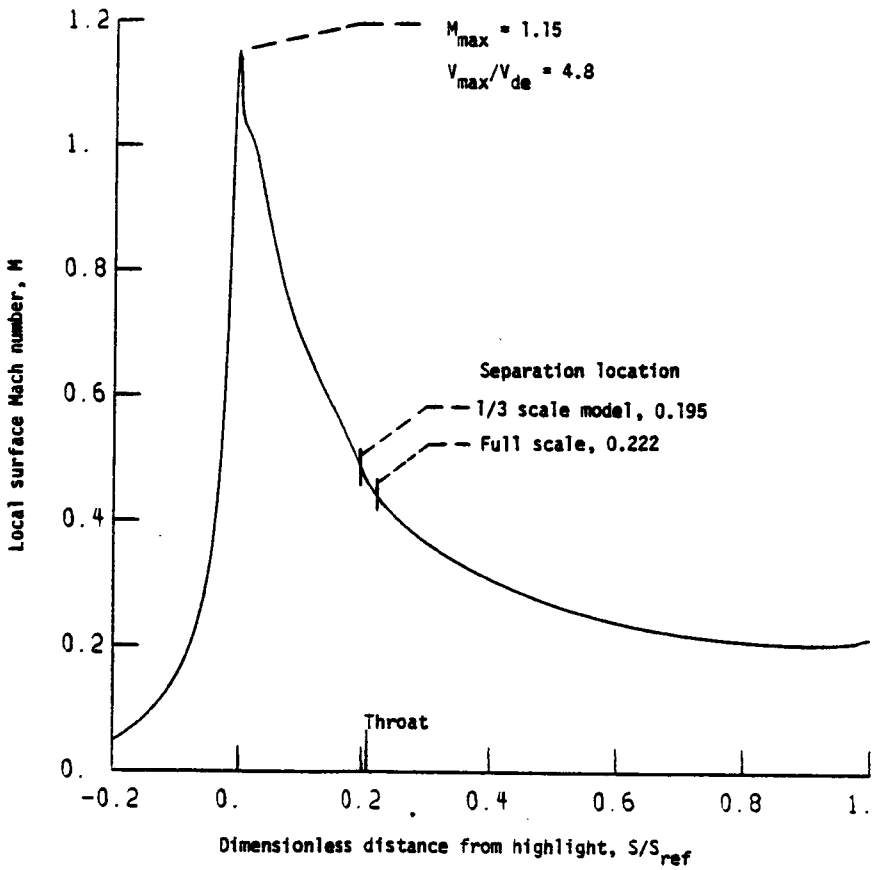

Figure 8. Theoretical local surface Mach number for the 1/3 scale model and full-scale inlets at the design point, incidence angle of 70°, free-stream Mach number of 0.18 and throat Mach number of 0.27.

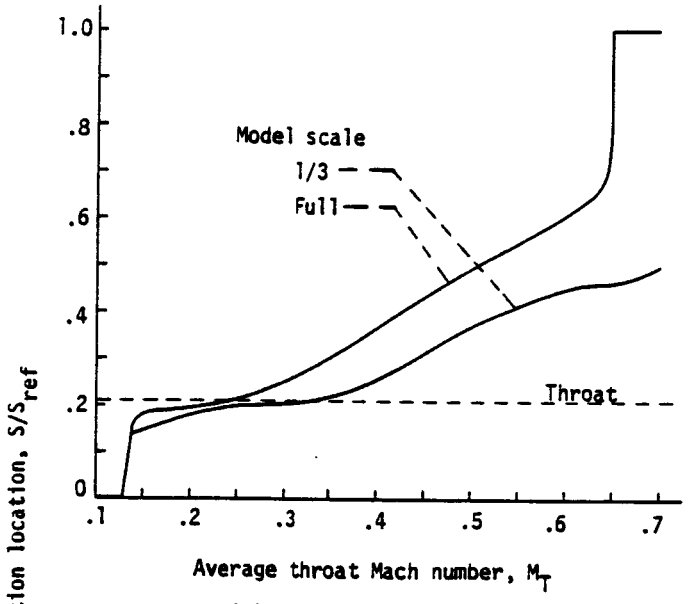

(a) Incidence angle, 70°

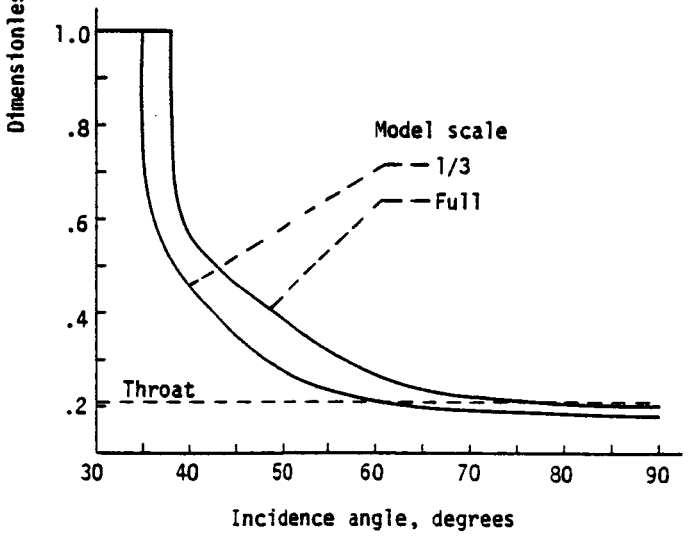

(b) Average throat Mach number, 0.27

Figure 9. Effect of average throat Mach number and incidence angle on separation location for 1/3 scale model and full-scale inlets. $M_0 = 0.18$.

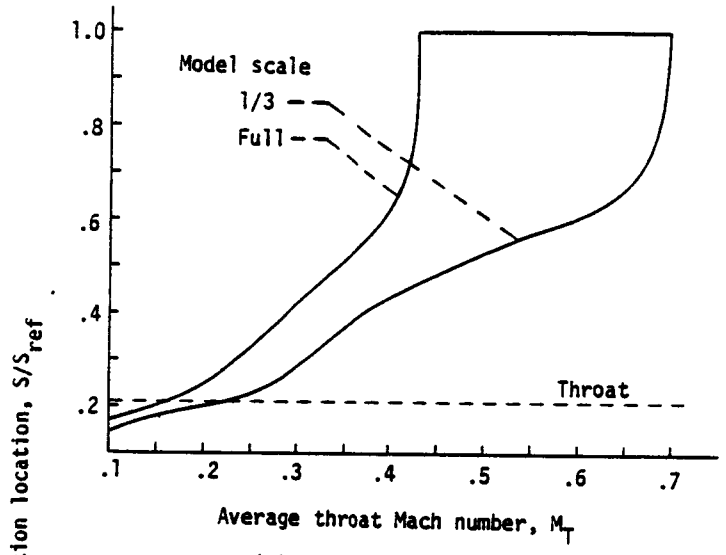

(a) Incidence angle, 70°

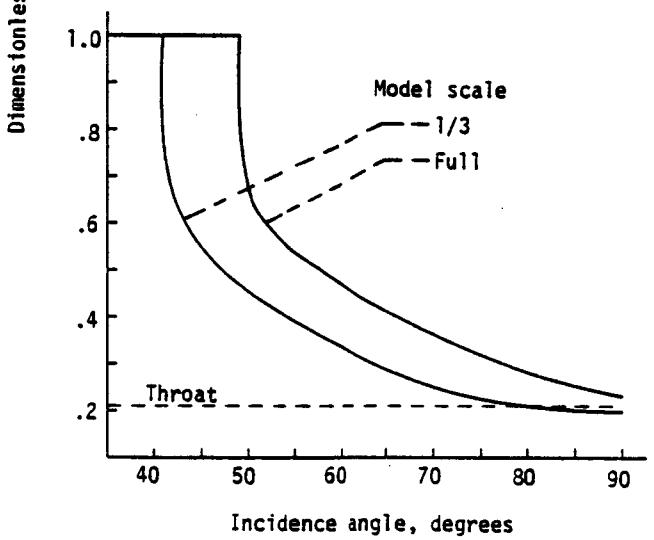

(b) Average throat Mach number, 0.27

Figure 10. Effect of average throat Mach number and incidence angle on separation location for 1/3 scale model and full-scale inlets. $M_0 = 0.12$

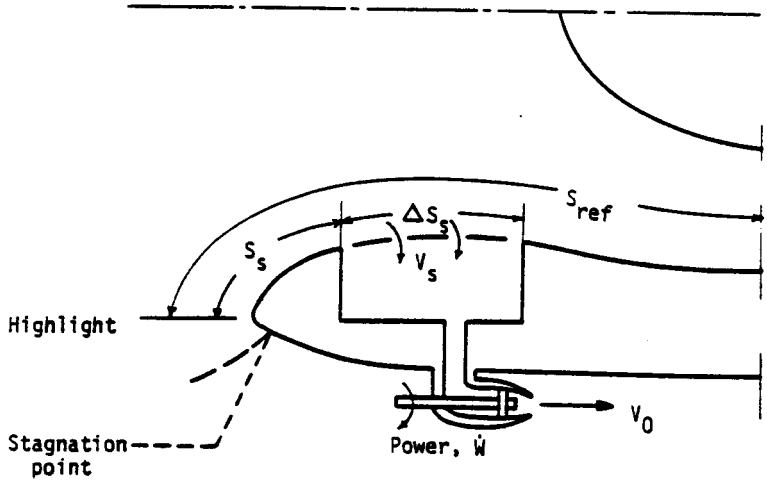

Figure 11. Suction boundary-layer control system

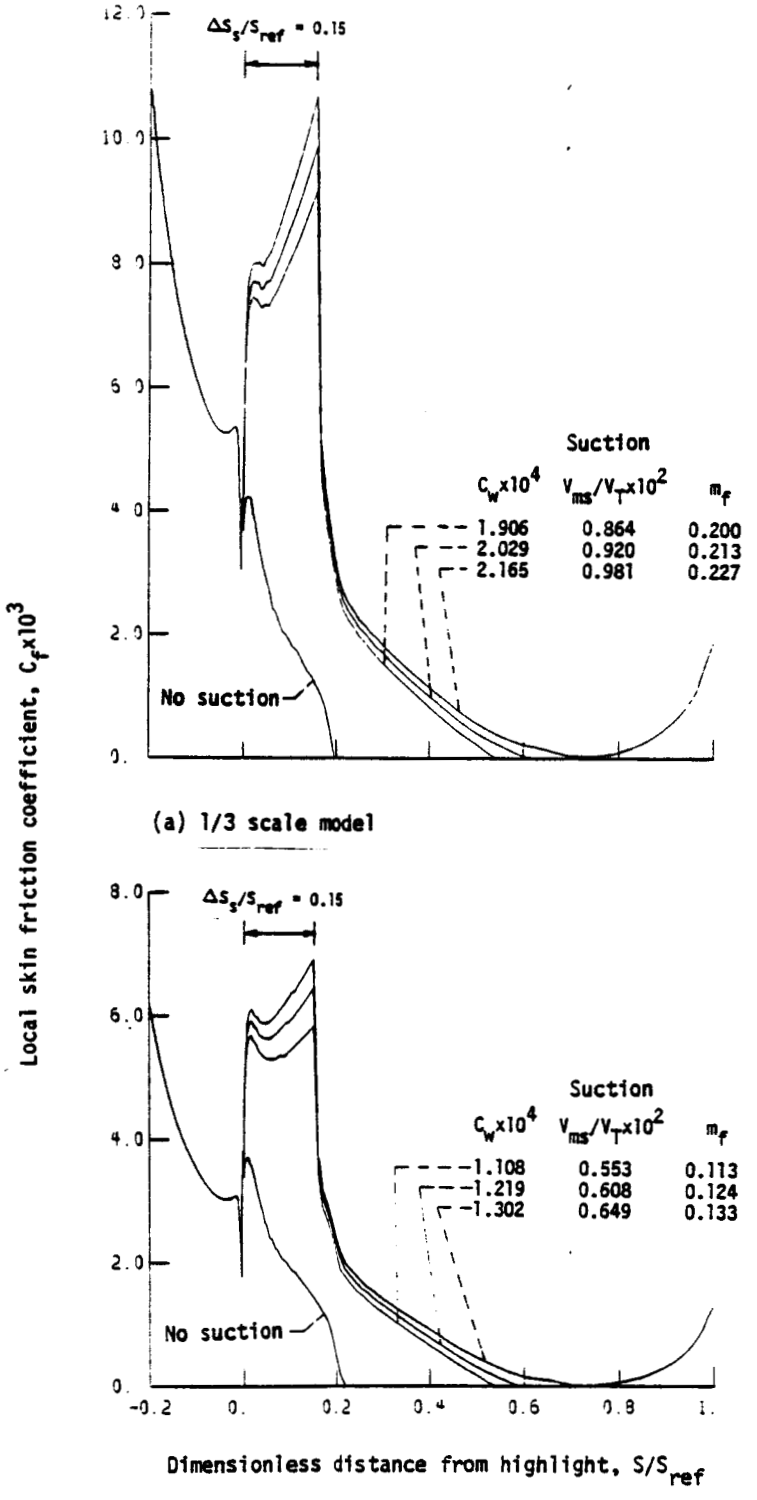

Figure 12. Effect of suction parameters on the local skin friction coefficient for 1/3 scale model and full-scale inlets at incidence angle of 70°, free-stream Mach number of 0.18 and average throat Mach number of 0.27 for suction location of S_s/S_{ref} = 0 and suction extent $\Delta S_s/S_{ref}$ = 0.15.

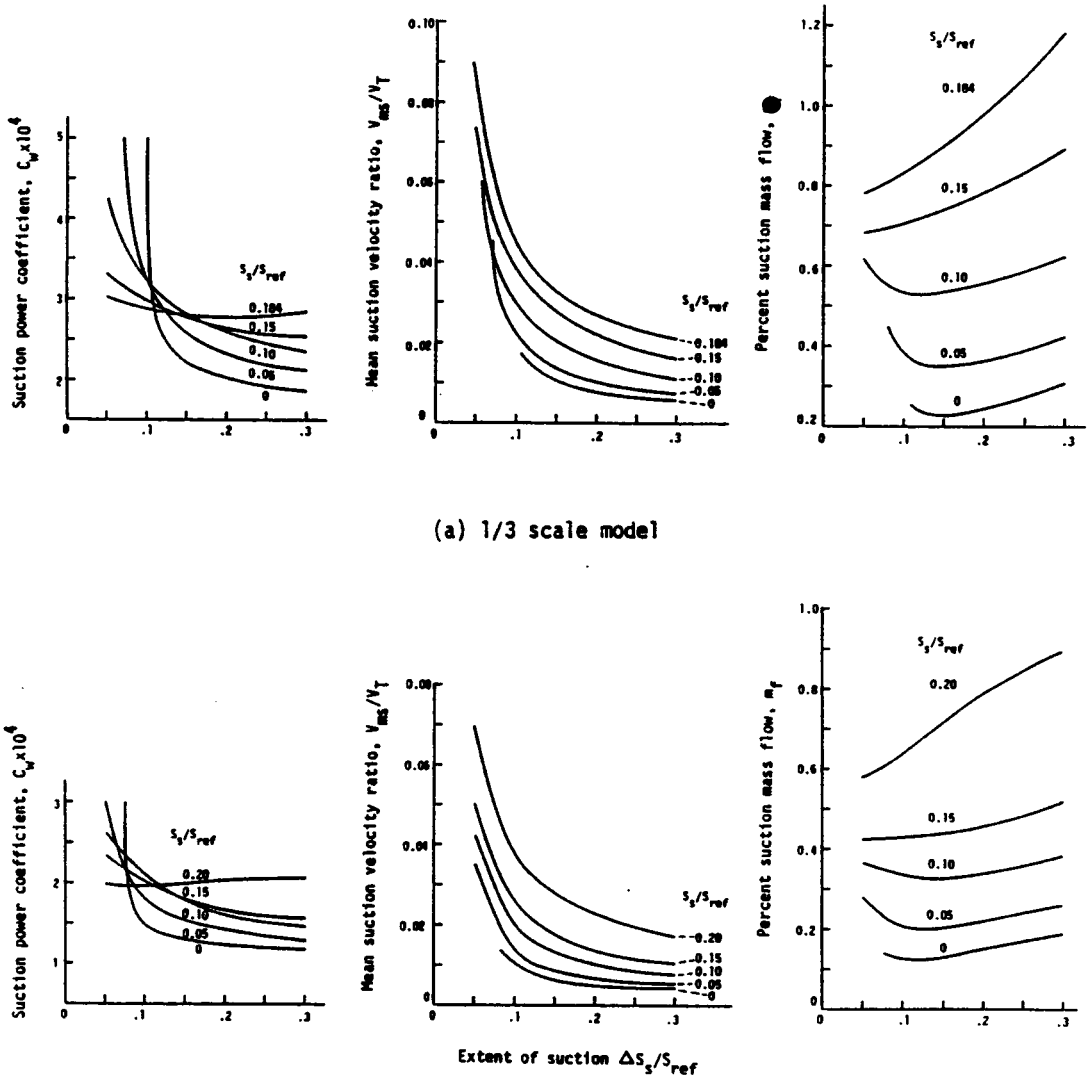

(a) 1/3 scale model

(b) Full scale

Figure 13. Effect of suction locaion and suction extent on suction power coefficient, mean suction velocity and percent suction mass flow for 1/3 scale model and full-scale inlets at incidence angle of 70°, free-stream Mach number of 0.18 and average throat Mach number of 0.27.

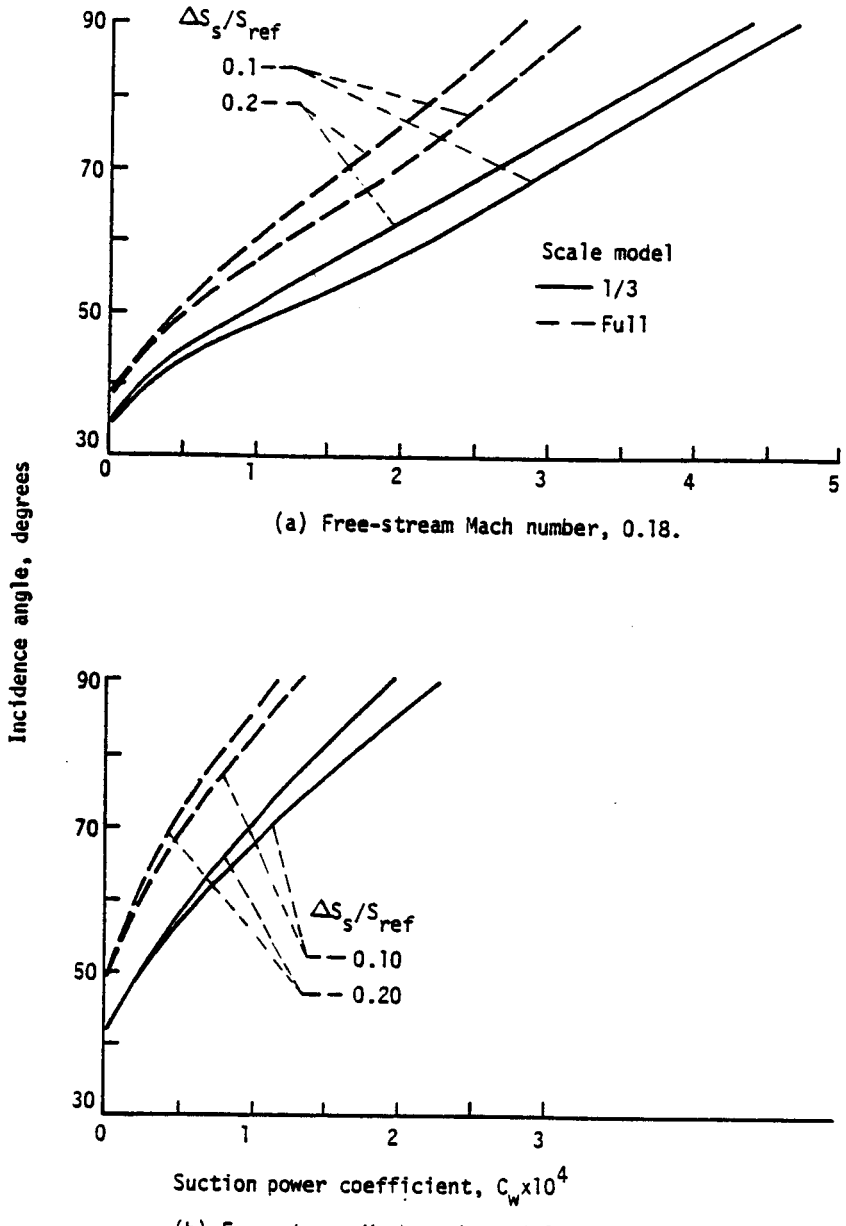

Figure 14. Variation of incidence angle with suction power coefficient for 1/3 scale model and full-scale inlets for suction location, S_s/S_{ref}, of 0.15, suction extent, $\Delta S_s/S_{ref}$, of 0.1 and 0.2. M_T = 0.27. M_0 = 0.12 and 0.18.

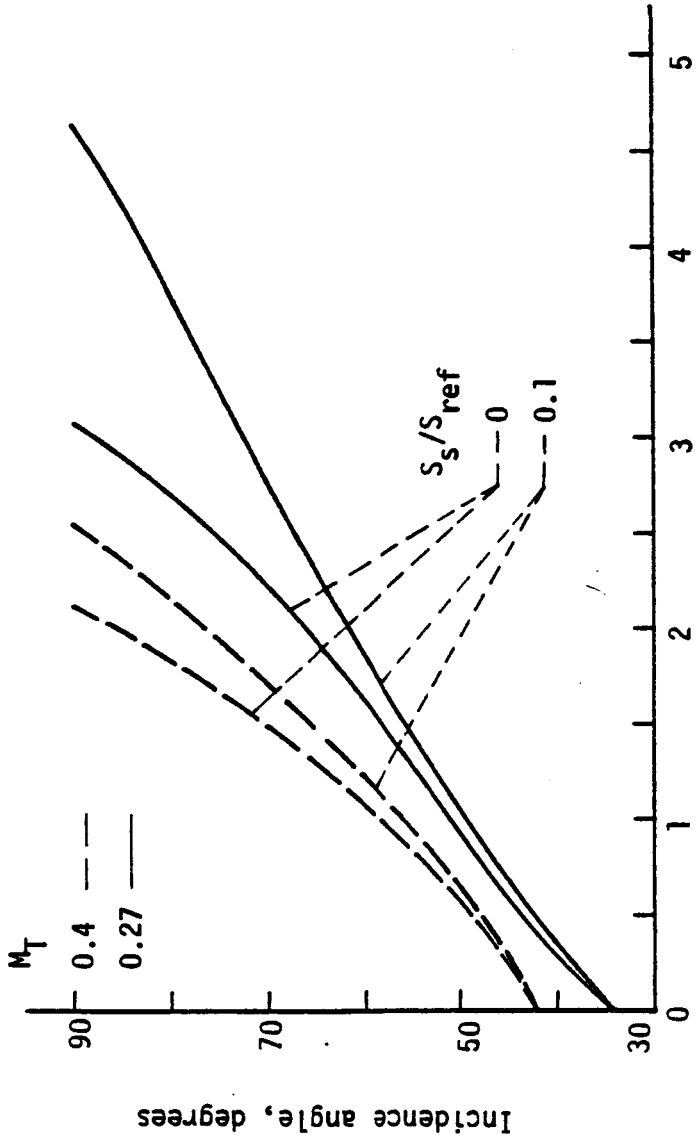

Figure 15. Effect of suction power coefficient on incidence angle for 1/3 scale model inlet for average throat Mach numbers of 0.27 and 0.4, free-stream Mach number of 0.18, suction extent of 0.15 and suction location, S_s/S_{ref}, of 0 and 0.1.